

Design and simulation of rectangular patch antenna arrays with high bandwidth for 2.4 GHz ISM band applications

Kymbat Kopbay, Madiyar Nurgaliyev, Ahmet Saymbetov, Nurzhigit Kuttybay, Askhat Bolatbek, Sayat Orynbassar, Batyrbek Zholamanov

Department of Electronics and Astrophysics, Faculty of Physics and Technology, Al-Farabi Kazakh National University, Almaty, Kazakhstan

Article Info

Article history:

Received Aug 31, 2024

Revised Feb 6, 2025

Accepted Mar 11, 2025

Keywords:

Ansys high frequency structure simulator

Impedance matching

Microstrip patch antenna array

Quarter-wave transformer

Wide bandwidth

ABSTRACT

Ongoing advancements in microstrip patch antenna (MPA) development research is driven by its compact size, cost-effectiveness and ease of fabrication. This paper presents a flexible design of patch antenna array (PAA) to address bandwidth (BW) limitations within the 2.4 GHz industrial, scientific, and medical (ISM) band, where narrow BW is a common challenge. To explore the effectiveness of different array configurations, we designed and evaluated 1×2 , 2×2 , and 2×4 element rectangular PAA, employing a quarter-wave transformer (QWT) method and parallel scheme for connecting patches. By utilizing Ansys high frequency structure simulator (HFSS) as the modeling environment, we conducted extensive simulations to refine the antenna parameters and achieve the most optimal MPA prototype. Our investigation demonstrates sufficiently good results, including BWs of 290 MHz and 210 MHz for 2×2 and 2×4 PAAs respectively, which account for 8.75% and 12% of the total value. The parameter return loss (RL) (S_{11}) reached -51dB for single-element patch antenna (SPA) and -37.5 dB for 8-element PAA, that shows an ideal impedance matching. In addition, the designed 2×4 PAA exhibited impressive performance metrics, accounting for 9.17 dB in gain, 13 dBi in directivity, and voltage standing wave ratio (VSWR) maintained below 0.5, ensuring excellent signal transmission and reception.

This is an open access article under the [CC BY-SA](#) license.



Corresponding Author:

Madiyar Nurgaliyev

Department of Electronics and Astrophysics, Faculty of Physics and Technology

Al-Farabi Kazakh National University

71 Al-Farabi Ave, Almaty, Kazakhstan

Email: nurgaliyev.madiyar@kaznu.kz

1. INTRODUCTION

In the fast-growing field of wireless communication systems, the need for efficient and compact antenna designs remains as a paramount issue [1], [2]. Among these, microstrip patch antennas (MPAs) have gained significant attention due to their compact dimension, easy fabrication, frequency-tuning flexibility, and seamless integration into various electronic devices [3], [4]. With their planar structure and relatively low profile, MPAs present an appealing solution for a broad range of applications, spanning from satellite communications to wireless sensor networks (WSNs) [5]–[8]. Despite numerous advantages, MPA also has some drawbacks such as narrow bandwidth (BW) and insufficient gain [9]. Additionally, there is a need to enhance its directivity for specific applications [10].

The diverse application requirements have led to a variety of patch antenna designs [11]–[16], with shapes ranging from rectangular, circular, and triangular to more complex geometries incorporating slots,

stubs, and truncated grounds. The development of a PAA involves grappling with a series of more intricate tasks compared to single-element patch antenna (SPA). Among these objectives, perhaps the most important is to optimize the antenna performance while maintaining optimal geometry and spacing between individual patch elements to achieve desired BW, directivity, and sidelobe levels. There are numerous works that were carried out to construct antenna arrays of various sizes and shapes [17]–[21]. Prakasam *et al.* [22], simulated and analyzed a 2×4 circular patch antenna array (PAA) with a center probe feed and FR-4 substrate. The design resulted in a 6.46% BW, a return loss (RL) (S_{11}) -16.5 dB, and a gain 8 dB at 2.4 GHz. One of the most critical aspects in probe feeding is to accurately place the pin rod connecting the patch with a microstrip line, and even the slightest deviations can disrupt impedance matching and totally alter the resonant frequency. However, in larger arrays, probe feeding facilitates uniform electromagnetic wave distribution through the transmission network. The rectangular 1×2 PAA based sector antenna for directional WSNs was proposed and fabricated in [23] with a measured maximum gain of 5.2 dBi, corresponding to the beamwidth of 45°. In order to connect individual patches, a corporate feeding technique (CFT), specifically a quarter-wave transformer (QWT) was employed. In article [24], the QWT technique was utilized to serially connect 2 and 4 element rectangular bow-tie patches, resulting in a 15.83% BW and a 13.6 dB gain for the 4-element PAA configuration.

In rural areas, there is a great demand for PAA for wireless communication applications. Therefore, Aji *et al.* [25] offered a 4×4 conventional rectangular PAA for remote regions using CFT with a probe and fabricated it using FR-4 substrate. Kaboutari *et al.* [26] examined how the impedance matching and radiation patterns (RPs) of arrays are affected by the quantity of elements in the array. They constructed an 8×2 square antenna array with a common feed and showed that its RP exhibits side lobes consistent with the cosecant-square curve. By employing a square shape and a daisy chain connection, they attained an average gain of 14.22 dBi and a wide impedance BW value of 1.93 GHz ranging from 9.97 to 11.90 GHz. Al-Yasir *et al.* [27] presents a new type of antenna filter having a relatively 50% BW, designed based on three types of dielectric substrates (Rogers RO3003, Rogers RT5880, and FR-4 epoxy), using the same design scheme at 2.4 GHz band. Although the wide BW is obtained, it can be noticed that the best performance was reached by using the Rogers RT5880, while antenna developed based on the FR-4 shows relatively little gain and matching.

This work aims to develop and analyze optimized, simplified design for a rectangular microstrip PAA to achieve wider BW, higher gain and improved impedance matching using cost-effective materials as FR-4 epoxy. We present the optimal design of the SPA model, as well as 1×2, 2×2, 2×4 PAA, where we achieved remarkable results by increasing the BW to 290 MHz, as well as reaching RL up to -30 dB through the high frequency structure simulator (HFSS) Ansys 3.0 modeling environment using FR-4 epoxy substrate material. The operating frequency was set to 2.4 GHz due to its particular relevance in the realm of wireless communication devices. This frequency band is globally allocated for industrial, scientific, and medical (ISM) applications, making it an appealing option for wireless communication standards [28]. Opting for FR-4 epoxy substrate instead of other alternatives as Rogers or RT/duroid is attributed to its cost-effectiveness, affordability and some mechanical properties, which make it a good solution for a various electronic applications.

2. METHOD

2.1. Single-element patch antenna geometry

2.1.1. Patch dimensions

The rectangular MPA stands out as the most optimal configuration among all available patch geometries, making it a popular choice for widespread use. It includes a radiating patch printed on a substrate made from dielectric material, backed by a ground plane [29]. The simplicity of its construction hides the potential for high performance across a wide range of frequencies. However, proper impedance matching is often a challenging task and every change in structure design considerably affects its basic characteristics, such as RL, RP, and voltage standing wave ratio (VSWR), and gain [30]. Therefore, it is crucial to choose the correct patch size, feed lines, ground surface, substrate thickness and placement of slots [31].

To develop the optimal MPA design, patch dimensions, substrate material and operating frequency should be defined. The dimensions of the patch antenna is a key parameter that influences its radiation diagram, impedance matching, resonant frequency, and so on. The equation that used for calculating width of the patch is presented in (1) [32]:

$$W = \frac{c}{2f_r} \sqrt{\frac{2}{\epsilon_r + 1}} \quad (1)$$

where, c represents the speed of light (3×10^8), f_r is the antenna's resonant frequency and ϵ_r denotes the substrate's dielectric permittivity. There are various substrates available for designing MPAs, such as FR-4, Rogers RT/Duroid, and Teflon (usually ϵ_r takes value from 2.2 to 12). The choice of substrate relies on several factors, including material cost, its thermal conductivity, dissipation coefficient, and others. In this article, we selected FR-4 epoxy, with relative dielectric constant as $\epsilon_r=4.4$ and substrate height of 1.6 mm.

In MPA, the patch width is typically chosen to be a fraction of the guided wavelength (λ_g) to manage its resistance. The λ_g of a patch antenna denotes the wavelength of the electromagnetic wave propagated through the microstrip transmission line formed by the patch and the ground plane. It is usually shorter than the free-space wavelength (λ) due to the dielectric properties of the substrate such as effective dielectric constant (ϵ_{eff}) and the operating frequency. The λ_g can be written as (2):

$$\lambda_g = \frac{\lambda}{\sqrt{\epsilon_{eff}}} = \frac{c}{f_r \sqrt{\epsilon_{eff}}} \quad (2)$$

The ϵ_{eff} considers how the substrate properties and the geometry of the patch influence on the overall electrical characteristics. It represents the average dielectric constant experienced by electromagnetic waves within the microstrip patch structure and is nearly close value to ϵ_r , but slightly less. In order to calculate ϵ_{eff} the following empirical equation is usually used:

$$\epsilon_{eff} = \frac{\epsilon_r + 1}{2} + \frac{\epsilon_r - 1}{2} \left[1 + \frac{12h}{W} \right]^{-1/2} \quad (3)$$

where, W is the width of the patch, and h is the substrate material height, which is usually defined as $h \ll \lambda$ ($0.003 \lambda \leq h \leq 0.005 \lambda$). The patch length can be expressed by (4):

$$L = \frac{c}{2f_r \sqrt{\epsilon_{eff}}} = \frac{\lambda_g}{2} \quad (4)$$

In the case of rectangular patch, the length (L) of the element typically falls within the range of $\frac{\lambda}{3} < L < \frac{\lambda}{2}$.

However, as radiation doesn't emanate from the center but rather from the region between the edges of the patch and the grounded surface, the phenomenon referred to as the fringing effect arises [33]. Consequently, electrically, the patch appears longer than its typically calculated length, giving rise to the concept of ΔL (Figure 1), which represents the extra electrical length.

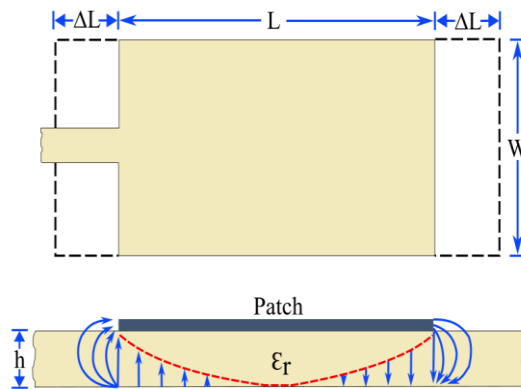


Figure 1. Physical and effective length of rectangular microstrip patch

A widely used and pragmatic approximate relationship for the normalized length elongation is:

$$\frac{\Delta L}{h} = 0.412 \frac{(\epsilon_{eff} + 0.3) \left(\frac{W}{h} + 0.264 \right)}{(\epsilon_{eff} - 0.258) \left(\frac{W}{h} + 0.8 \right)} \quad (5)$$

The patch effective length, denoted as L_{eff} , is given as (6):

$$L_{eff} = L + 2\Delta L \quad (6)$$

Designing a suitable ground plane under the patch antenna will improve radiation efficiency and maintain stable impedance. The dimensions of the grounding surface can be chosen by the subsequent expression:

$$L_g = L + 6h \quad (7)$$

$$W_g = W + 6h \quad (8)$$

2.1.2. Feeding calculation technique

Feeding mechanisms are used to transfer electromagnetic power from transmission line to the antenna by transforming energy into electromagnetic radiation. It plays a critical role in impedance matching and effects on basic characteristics such as RP, frequency and polarization. Common types of feeding mechanisms in patch antennas include microstrip, proximity, aperture coupled and coplanar waveguide configurations. Each of them has its own pros and cons, and the choice depends on factors such as antenna design requirements, performance goals, and application constraints.

In this article, the microstrip edge feed was favored for its design simplicity and ease fabrication, which involves connecting a transmission line straight to the edge of the patch antenna. With any feeding technique, achieving accurate impedance matching is vital as it minimizes signal reflections and standing waves, while maximizing the power transfer efficiency. By adjusting the width and length of the transmission line, impedance matching can be optimized.

The width and length of the patch are calculated by (1) and (6), so that $W_p = 37.1$ mm and $L_p = 27.7$ mm, respectively. In order to define and calculate the feeding size, it is necessary to determine the load impedance (Z_L) of the patch through (9):

$$Z_L = 90 * \frac{\epsilon_r^2}{\epsilon_r - 1} \left(\frac{L}{W}\right)^2 \quad (9)$$

Thus, when substituting values into (9), $Z_L \approx 285$ ohms. The calculation of the reflection coefficient Γ , provided that the characteristic impedance (Z_0) is 50 ohms, is carried out using (10):

$$\Gamma = \frac{Z_L - Z_0}{Z_L + Z_0} \quad (10)$$

From (10), a value of $\Gamma=0.7$ is determined, which indicates that 70% of the incident power at the antenna's feed point is reflected back towards the source, and the remaining 30% is either absorbed or radiated by the antenna. The value of $\Gamma=0.7$ indicates poor impedance matching, whereas ideal matching is characterized by a reflection coefficient close to zero. To minimize the reflection coefficient, we employ matching technique as QWT, which adjusts the antenna's impedance to match the characteristic impedance of the feeding transmission line. The phase and magnitude of the reflected signal is transformed to diminish the reflection coefficient. To calculate QWT impedance (Z_t) we will use (11):

$$Z_0 = Z_t \frac{Z_L + jZ_t \tan(\beta l)}{Z_t + jZ_L \tan(\beta l)} \quad (11)$$

Since in the matching network $l = \lambda/4$ (as shown in Figure 2), it implies that $\beta l = \frac{2\pi}{\lambda} \frac{\lambda}{4}$. As a result, it is evident that $\tan(\frac{\pi}{2}) \rightarrow \infty$, leading to (11) being expressed as (12):

$$Z_0 = \frac{Z_t^2}{Z_L}, Z_t = \sqrt{Z_0 Z_L} \quad (12)$$

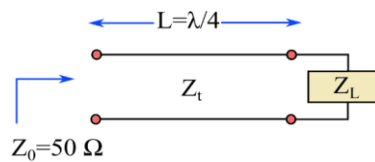


Figure 2. QWT

Hence, we can figure out the length of QWT by expression $L_t = \frac{\lambda}{4}$.

The width of the QWT and microstrip feed with a 50Ω characteristic impedance can be determined using (13):

$$Z_c = \begin{cases} \frac{60}{\sqrt{\epsilon_r}} \ln \left(\frac{8h}{W} + \frac{W}{4h} \right), & \frac{W}{h} < 1 \\ \frac{120\pi}{\sqrt{\epsilon_r} \left(1.393 + \frac{W}{h} + \frac{2}{3} \ln \left(\frac{W}{h} + 1.444 \right) \right)}, & \frac{W}{h} > 1 \end{cases} \quad (13)$$

Figure 3 illustrates the geometric structure and key parameters of the rectangular SPA design, including the dimensions of the patch, transformer, microstrip feed, and substrate. These labeled parameters form the basis for the modeling and simulation discussed in this article. Table 1 provides the specific width and length values corresponding to each parameter depicted in Figure 3. Since the design relies on empirical equations, slight adjustments to these values may be necessary to achieve optimal performance in practical implementations.

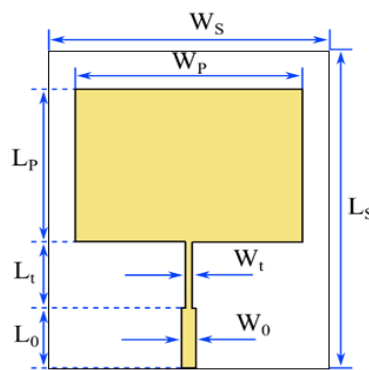


Figure 3. Rectangular single MPA

Table 1. The parameters of rectangular single patch antenna design

Symbols	Details	Value (mm)
W_s	Substrate width	48
L_s	Substrate length	66
W_p	Patch width	37.1
L_p	Patch length	27.7
W_t	Width of transformer	1.2
L_t	Length of transformer	15
W_0	Width of microstrip line feed (50 Ohm)	2.98
L_0	Length of microstrip line feed (50 Ohm)	15.5
H	Height of substrate	1.6

2.2. Patch antenna array geometry

In specific scenarios, the desired traits of an antenna can be accomplished using just one microstrip element. Nevertheless, similar to traditional microwave antennas, features like high gain, wide BW, and beam direction control are only achievable by combining separate radiators into volumetric arrays. The components may be arranged in series, parallel or by diagonal to form an array. In practical terms, the selection of its configuration depends on the applications' characteristics.

In this paper, we have gathered PAA of varying configurations, including 1×2 , 2×2 , 2×4 elements, to ensure a more equitable comparison of the results. Each individual patch dimension coincides with the information indicated in Table 1. In the 1×2 line array, the spacing between patches is determined based on the guided wavelength λ_g , which is equal to 59.1 mm. A matching network with impedances Z_1 , Z_2 , Z_3 are used to provide effective and smooth transition. This is essential because employing only a single line with a fixed impedance value to connect two distinct patches often leads to significant power reflection, thereby causing inadequate matching. To resolve this concern, we employ the QWT method relying on (12). Also, as

it can be seen from Figure 4(a), the wavelength between the patches is divided into fractions equal to $\lambda/6$, $\lambda/4$ and $\lambda/2$ (the section lengths used in the simulation may slightly differ from the theoretical data, in order to reach the best matching). The width and length of matching network transformers are given in Table 2.

Table 2. The parameters of matching network feed

Impedances	Width of feed (mm)	Length of feed (mm)
Z_1	2.98	10.2
Z_2	1.54	7.6375
Z_3	1.2	23.425
Z_0	2.98	15.5

When constructing a 4-element PAA, the identical circuit is used as in a 2-element PAA; 2 similar patches are added in parallel, which are located at a distance of 48.7 mm from the top ones (Figure 4(b)). To enhance the performance characteristics of the antenna array, the distance between the upper and lower antennas should be reduced to less than the wavelength, specifically $0.82 \lambda_g$ in this case. The radiation elements are energized through a common feedline, which guarantees an even distribution of power among them. The same steps are performed when creating an 8-element PAA. In order to connect 2 sides of an array consisting of 4 elements, we need to use conductor line with a length of $2 \lambda_g$ (Figure 4 (c)).

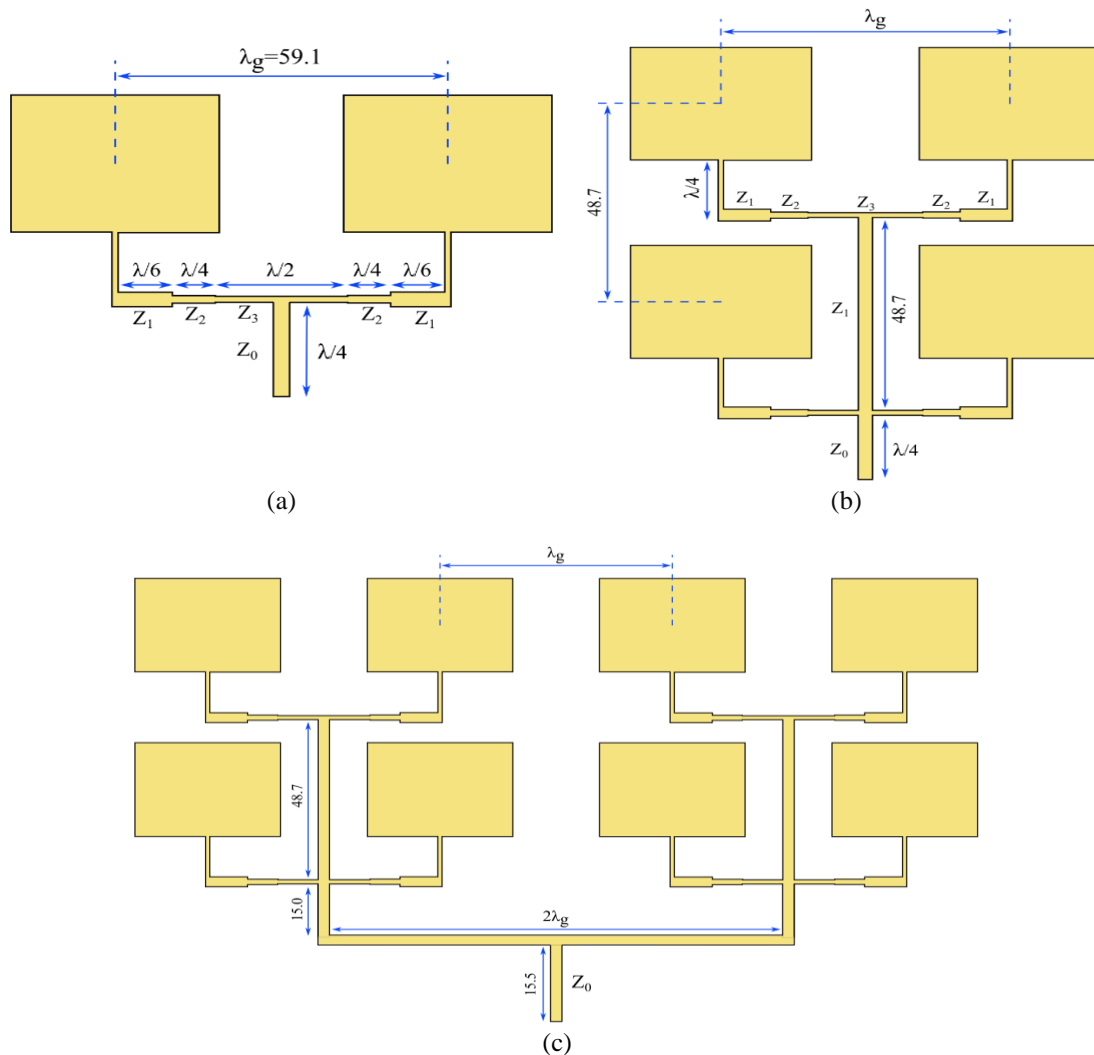


Figure 4. The front side of; (a) 1×2 PAA, (b) 2×2 PAA, and (c) 2×4 PAA

3. RESULTS AND DISCUSSION OF ANTENNA DESIGN SIMULATIONS

The simulation of proposed SPA and PAA was accomplished by utilizing the Ansys HFSS 3D modeling software product. The operating frequency of the antenna is chosen to be $f_r = 2.4$ GHz, the substrate material is FR-4 and dielectric constant $\epsilon_r = 4.4$. Following that, we compare the simulation results of 1, 2, 4, and 8-element patches, namely parameters as RL (S_{11}), BW, gain, VSWR, directivity, and 2D, 3D RPs.

3.1. Return loss (S_{11}), bandwidth, and voltage standing wave ratio

In the field of antenna engineering the S_{11} value is a crucial metric as it quantifies how effectively the antenna transforms incoming signal energy into radiated waves versus reflecting it back into the system. Lower values of S_{11} denote superior impedance matching between the antenna and transmission line, translating to reduced signal loss and enhanced overall performance.

As depicted in Figure 5(a), the S_{11} parameter of SPA reached the highest point as -51.7 dB at the resonant frequency, indicating perfect matching without any signal reflections. Similarly, the S_{11} results do not differ significantly in the 2-element PAA (Figure 5(b)), achieving -47.5 dB at 2.4 GHz. Both types of antennas have a BW of 60 MHz, which is considered as a relatively narrow frequency band. Subsequently, by utilizing a parallel patch addition scheme and optimizing patch placements based on the model, a 4-element PAA (Figure 5(c)) attained a BW of 290 MHz at -10 dB, with an increased number of resonant frequencies observed at 2.28 GHz (S_{11} : -17.8 dB), 2.39 GHz (S_{11} : -25.5 dB), and 2.49 GHz (S_{11} : -30.6 dB). The 8-element PAA exhibits multiple resonant frequencies, as shown in Figure 5(d). At 2.46 GHz, S_{11} drops to -37.3 dB, while at 2.25 GHz, it reaches -21.6 dB. The BW covers range from 2.22 to 2.29 GHz and 2.36 to 2.5 GHz, giving a total BW of 210 MHz.

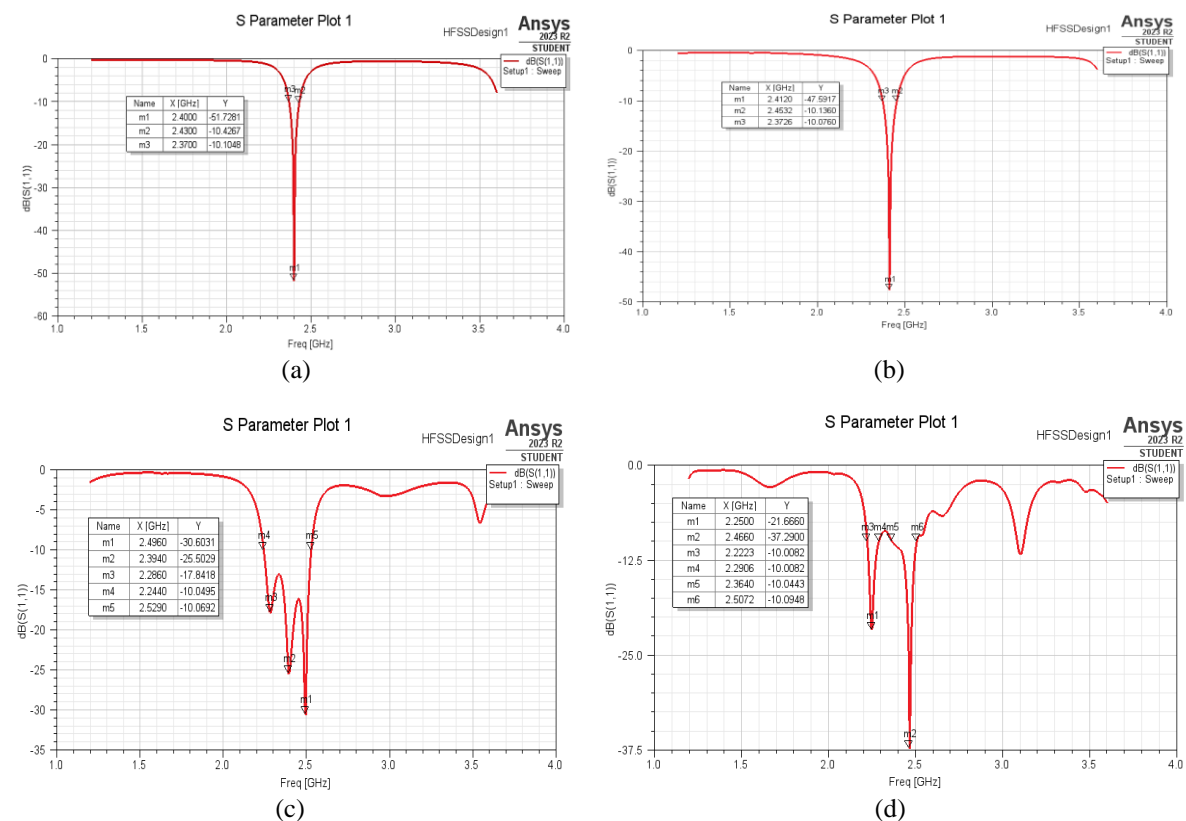


Figure 5. The S_{11} parameter and BW of; (a) SPA, (b) 1×2 PAA, (c) 2×2 PAA, and (d) 2×4 PAA

VSWR is directly related to RL, because they are inversely proportional. Higher S_{11} value corresponds to lower VSWR, and vice versa. Lower VSWR indicates better impedance matching and less power being reflected back towards the source. As it can be seen from Table 3, we obtained VSWR values for SPA which is only 0.04, and also for 8-element PAA values of 0.23, indicating high signal transmission efficiency.

Kaboutari *et al.* [26] constructed a 2×2 circular PAA using a probe feed, where connections between individual patches are similar to our proposed approach. The distinction lies not only in the shape of the patch, but also in the connection type, as we employ edge-feed supply instead of probe feed. Compared to the circular PAA, which achieved only 3.65% of the BW in the frequency range from 2.37 GHz to 2.45 GHz, our 2×2 rectangular PAA increased the BW by 12% in the 2.21-2.53 GHz frequency range. Additionally, S_{11} , VSWR, and gain value are recorded at -15.19 dB, 1.4885, and 6.75 dBi, correspondingly. In comparison, the proposed rectangular 2×2 PAA demonstrates results as -30.6 dB for S_{11} , 0.5 for VSWR, and 7.08 dBi for gain. Aji *et al.* [25] presented a 4×4 rectangular PAA fed by a microstrip line, designed for wireless applications in rural regions, demonstrating a BW of 130 MHz. Our study proposes a 2×4 PAA that exceeds this result, reaching a BW of 210 MHz, constituting 8.5% of the total available BW.

Table 3. Various obtained model data of 1, 2, 4, and 8-element PAA

Parameter	Number of patch elements			
	1	2	3	4
Resonant frequency (GHz)	2.4	2.4	2.49	2.46
RL (dB)	-51.7	-47.5	-30.6	-37.3
Gain (dB)	2.64	6.03	7.08	9.17
BW (MHz)	60	60	290	210
VSWR	0.04	0.07	0.5	0.23
Directivity (dBi)	5.96	8.8	10.48	13.13
HPBW (°) (E plane)	83 [-37; 46]	89 [-40; 49]	52 [-5; 57]	61 [4; 65]

3.2. Radiation pattern, gain, and directivity

Antenna gain (G) is a crucial parameter that describes the concentration of the antenna's RP. It combines the directivity (D) and efficiency (η) of the antenna into a single, convenient value. Directivity measures the ratio of power density (radiation intensity per unit area) of a real antenna in its main radiation direction to that of a hypothetical isotropic antenna, which radiates evenly in all directions. In contrast, the power density of an isotropic emitter is uniformly distributed across the surface of a sphere. A real antenna, however, exhibits varying degrees of radiation directivity, which is quantitatively represented by the directivity coefficient. The equation for calculating directivity is as (14):

$$D = \frac{S}{S_i} \quad (14)$$

where, S represents the power density of the real antenna in its primary radiation direction, and S_i is the isotropic antenna's power density. While antenna directivity is a key aspect of antenna gain, real-world losses must also be considered. The power radiated by the antenna depends on the power received from the transmitter, which can be measured at the antenna feed. However, some power is lost along the supply line due to its ohmic resistance, impacting the antenna's efficiency. In the case of an ideal, lossless antenna, gain equals directivity. For real practical antennas, the value of gain is always less than the directivity:

$$G = \eta D \quad (15)$$

In order to see the full picture of the received data, we use the RP extracted through far-field analysis in Ansys HFSS. We obtained 3D models of gain, encompassing azimuth angle (φ) values ranging from -180° to 180° and elevation angle (θ) values ranging from 0° to 360° (Figure 6). The 3D RP of SPA exhibits a uniformly round distribution, which suggests symmetrical radiation characteristics with minimal variation in intensity around the antenna's axis. The gain and directivity value of SPA reached 2.64 dB and 5.96 dBi, respectively. In the case of 1×2 PAA configuration, we obtained substantially strong gain of 6.03 dB, along with directivity of 8.80 dBi. The presented three-dimensional RP in Figure 6(a) demonstrates that the SPA exhibits a relatively broad main lobe, with a peak gain of approximately 2.64 dB, as indicated by the red region. This pattern serves as a baseline for evaluating the improvements achieved with phased array configurations. As shown in the RP of Figure 6(b), a noticeable level of radiation is still present in the back lobe, although the overall gain has significantly increased. Specifically, the gain reaches 7.08 dB for the 2×2 phased antenna array (PAA) and further improves to 9.17 dB for the 2×4 PAA, as illustrated in Figures 6(c) and 6(d). These enhancements are accompanied by an increase in antenna directivity, reaching up to 13.13 dBi, indicating improved beam focusing and overall performance.

Aji *et al.* [25] endeavored to enhance gain and directivity by using proximity feeding for 1×2 circular PAA, resulting in a 6.46 dBi gain and a directivity 7.59 dBi. In our study involving a 1×2 PAA, although we attained a slightly lower gain of 6.03 dBi, the directivity was higher than the circular PAA,

reaching 8.8 dBi. Balanis [32] created a sectored antenna with eight sides, each equipped with inset-feed 1×2 PAA's. They achieved a gain 5.83 dBi, a RL -29.7 dB, and a beamwidth 45° , all while maintaining a $\lambda/2$ spacing between patches. In the proposed design of the 1×2 PAA, we accomplished a higher gain 6.03 dBi, a RL -47 dB and a broader beamwidth due to the spacing between patches, which corresponds to λ .

Also, Kaboutari *et al.* [26] offers a 1×4 microstrip rectangular PAA with inset-fed feeding technique for WiMax applications. As a result of employing the corporate feeding arrangement, the authors obtained a maximum gain of 5.28 dBi and an S_{11} parameter of -20.37 dB. In contrast, the 2×2 PAA configuration proposed in this paper exhibited higher gain and S_{11} values of 7.08 dBi and -30.6 dB, respectively.

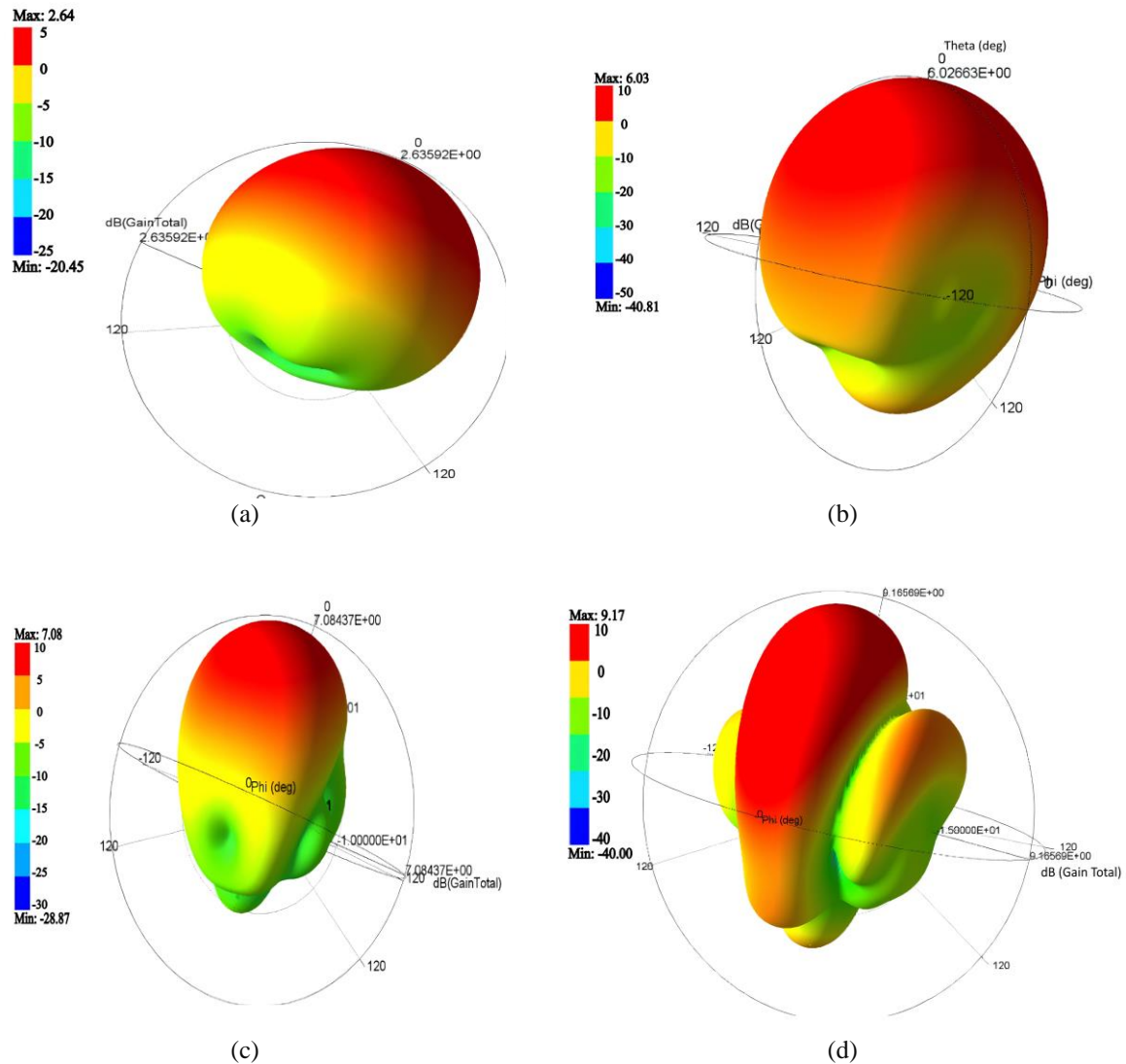


Figure 6. The RP 3D model of; (a) 1×1 , (b) 1×2 PAA, (c) 2×2 PAA, and (d) 2×4 PAA

Using a 3D polar plot, we can visualize how an antenna emits beams in 3D space, whereas a 2D plot is useful for accurately defining directivity and angles of emission since it represents a cross-section of the 3D pattern. The 2D RP of the SPA is described by a half-power beamwidth (HPBW) of 83° (Figure 7(a)), indicating the angular span within which the radiation intensity decreases to half (-3 dB) of the peak value. In the 1×2 PAA's scenario, the 2D plot demonstrates an even gain distribution and wide radiation angle similar to SPA with HPBW value spanning 88° from -40° to 49° (Figure 7(b)). Additionally, a more pronounced sidelobe and back lobe was observed from the H plane in the 2-element PAA. It can be noticed that the H plane in each plot has a similar trend, where increasing the number of patches leads to a reduction in the width of the main lobe and the appearance of additional sidelobes. For 2×2 and 2×4 element PAA

configurations, the E plane exhibits a more focused main lobe with a HPBW of 52° ranging from -5° to 57° and 61° spanning from 4° to 65° , respectively (Figures 7(c) and (d)).

All the data acquired during modeling, including gain, RL, VSWR, directivity, and other parameters, are showcased in Table 3. The animation of how electric field strength is propagated through the media in 2×4 PAA is presented in Figure 8. As observed from simulation, the surface current is uniformly propagated in two directions from the lower side of the patch antenna. However, there is a slight phase shift between the upper and lower groups of patches.

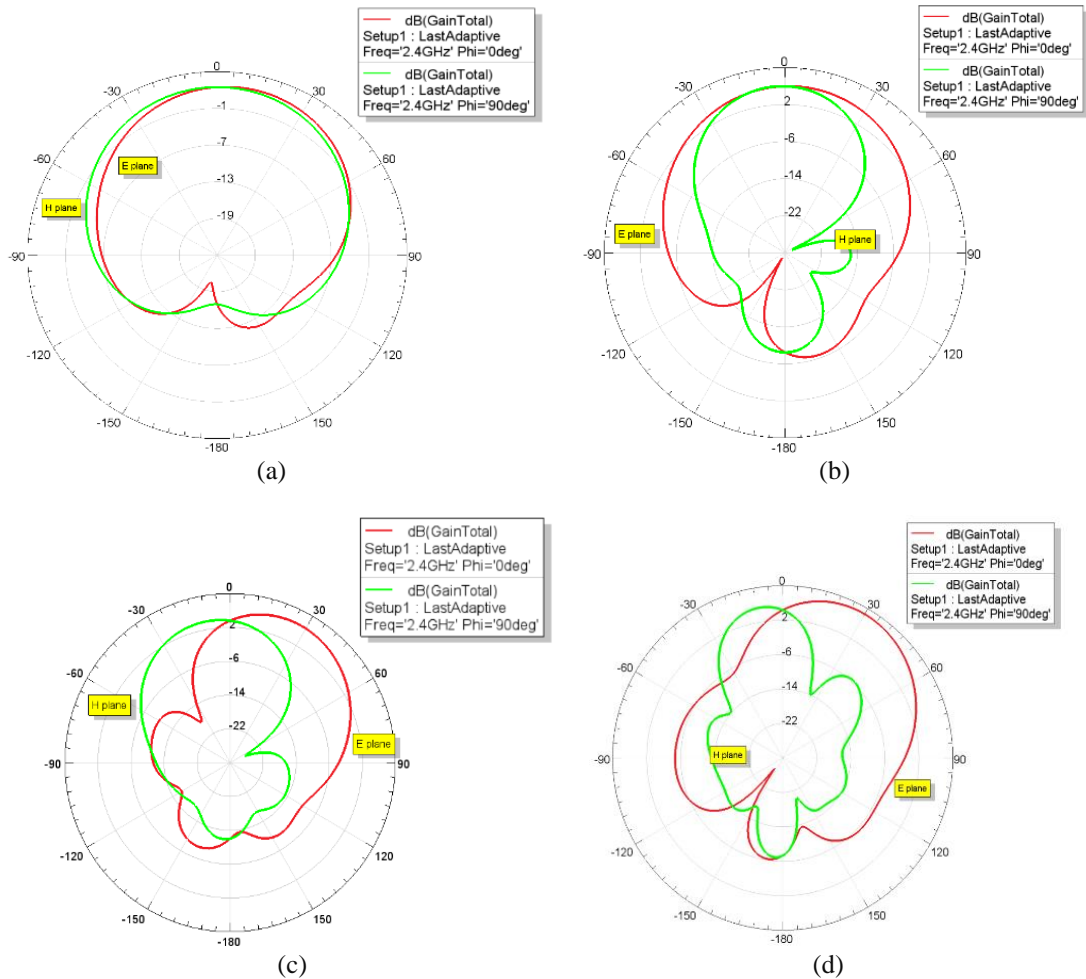


Figure 7. The 2D RP of E-plane ($\phi=0^\circ$) and H-plane ($\phi=90^\circ$); (a) 1×1 , (b) 1×2 PAA, (c) 2×2 PAA, and (d) 2×4 PAA

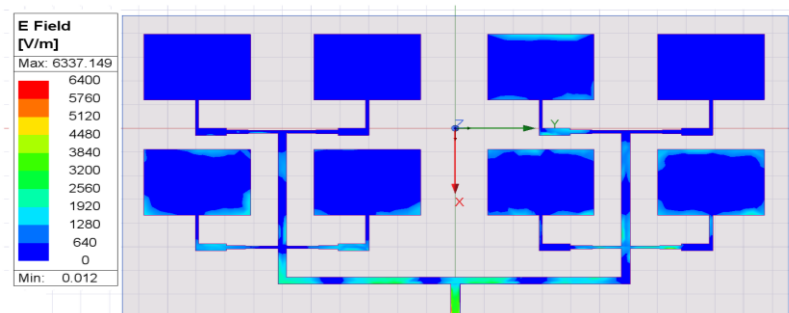


Figure 8. The E field animation of 2×4 PAA in phase from 0° to 180° degree

4. CONCLUSION

This work presented a straightforward and effective design of PAA consisting of 2-, 4-, and 8-elements in a rectangular shape for 2.4 GHz ISM band. For this purpose, it was proposed to use a QWT and parallel adding scheme with edge-feeding technique. As a result, there was a significant improvement in overall BW by 290 MHz, which is considered as 12% of total BW. The simulation results illustrate that the proposed architecture exhibited impressive values for RL (S_{11}) at -37.3 dB and VSWR at 0.23, indicating excellent impedance matching. The maximum achievable gain and directivity were measured at -9.17 dB and 13.13 dB respectively for the 2×4 PAA configuration. By examining the RPs in 2D and 3D polar plots, it was found that directivity enhances with an increase in the number of patch antenna elements. The proposed PAA design offers seamless integration and is ideal for various wireless communication applications.

ACKNOWLEDGEMENTS

The authors would like to express their sincere gratitude to Al-Farabi Kazakh National University for providing the resources and support necessary for this research. Special thanks are extended to the Department of Electronics and Astrophysics for their valuable guidance and collaboration.

FUNDING INFORMATION

This research has been funded by the Science Committee of the Ministry of Science and Higher Education of the Republic of Kazakhstan (Grant AP19678552).

AUTHOR CONTRIBUTIONS STATEMENT

This journal uses the Contributor Roles Taxonomy (CRediT) to recognize individual author contributions, reduce authorship disputes, and facilitate collaboration.

Name of Author	C	M	So	Va	Fo	I	R	D	O	E	Vi	Su	P	Fu
Kymbat Kopbay	✓	✓	✓		✓	✓		✓	✓	✓	✓			
Madiyar Nurgaliyev	✓	✓	✓	✓		✓		✓	✓	✓		✓	✓	
Ahmet Saymbetov	✓			✓			✓			✓		✓	✓	
Nurzhigit Kuttybay		✓			✓					✓	✓			
Askhat Bolatbek					✓		✓			✓				
Sayat Orynbassar	✓		✓					✓	✓	✓	✓			
Batyrbek Zholamanov	✓					✓			✓	✓				

C : **C**onceptualization

M : **M**ethodology

So : **S**oftware

Va : **V**alidation

Fo : **F**ormal analysis

I : **I**nterpretation

R : **R**esources

D : **D**ata Curation

O : **O**riginal Draft

E : **E**diting

Vi : **V**isualization

Su : **S**upervision

P : **P**roject administration

Fu : **F**unding acquisition

CONFLICT OF INTEREST STATEMENT

We confirm this manuscript has not been published elsewhere and is not under consideration by another journal. The authors have no conflicts of interest to declare.

DATA AVAILABILITY

The authors confirm that the data supporting the findings of this study are available within the article.




REFERENCES

- [1] D. Piao and Y. Wang, "Tripolarized MIMO antenna using a compact single-layer microstrip patch," *IEEE Transactions on Antennas and Propagation*, vol. 67, no. 3, pp. 1937-1940, Mar. 2018, doi: 10.1109/TAP.2018.2889147.
- [2] B. Mishra, R. K. Verma, N. Yashwanth, and R. K. Singh, "A review on microstrip patch antenna parameters of different geometry and bandwidth enhancement techniques," *International Journal of Microwave and Wireless Technologies*, vol. 14, no. 5, pp. 652-673, Jun. 2022, doi: 10.1017/S1759078721001148.
- [3] S. K. Ezzulddin, S. O. Hasan, and M. M. Ameen, "Microstrip patch antenna design, simulation and fabrication for 5G




- applications." *Simulation Modelling Practice and Theory*, vol. 116, p. 102497, Apr. 2022, doi:10.1016/j.simpat.2022.102497.
- [4] K. F. Lee, and K. F. Tong, "Microstrip patch antennas—basic characteristics and some recent advances," in *Proceedings of the IEEE*, vol. 100, no. 7, pp. 2169–2180, Jul. 2012, doi: 10.1109/JPROC.2012.2183829.
 - [5] K. Hati, N. Sabbar, A. El. Hajjaji, and H. Asselman, "A novel multiband patch antenna array for satellite applications," *Procedia Engineering*, vol. 181, pp. 496–502, May 2017, doi: 10.1016/j.proeng.2017.02.422.
 - [6] A. S. Elkorany *et al.*, "Implementation of a miniaturized planar tri-band microstrip patch antenna for wireless sensors in mobile applications," *Sensors*, vol. 22, no. 2, p. 667, Jan. 2022, doi: 10.3390/s22020667.
 - [7] D. B. Thi and T. H. T. Phuong, "A narrow beam steering antenna array for indoor positioning systems based on wireless sensor network," *IEEE Access*, vol. 10, pp. 2169–3536, Aug. 2022, doi: 10.1109/ACCESS.2022.3200594.
 - [8] C. Sun, "A design of compact ultrawideband circularly polarized microstrip patch antenna," *IEEE Transactions on Antennas and Propagation*, vol. 67, no. 9, pp. 6170–6175, Jun. 2019, doi: 10.1109/TAP.2019.2922759.
 - [9] S. Parasuraman, S. Yogeewaran, and G. P. Ramesh, "Design of Microstrip Patch Antenna with improved characteristics and its performance at 5.1 GHz for Wireless Applications," in *IOP Conference Series: Materials Science and Engineering: 1st ICCEMS*, vol. 925, no. 012005, Jul. 2020, doi: 10.1088/1757-899X/925/1/012005.
 - [10] M. Sağık *et al.*, "Optimizing the gain and directivity of a microstrip antenna with metamaterial structures by using artificial neural network approach," *Wireless Personal Communications* vol. 118, pp. 109–124, Jan. 2021, doi: 10.1007/s11277-020-08004-8.
 - [11] S. S. Hao, Q. Q. Chen, J. Y. Li, and J. Xie, "A high-gain circularly polarized slotted patch antenna," *IEEE Antennas and Wireless Propagation Letters*, vol. 19, no. 6, pp. 1022–1026, June 2020, doi: 10.1109/LAWP.2020.2987330.
 - [12] A. Romputtal and C. Phongcharoenpanich, "T-Slot Antennas-Embedded ZigBee Wireless Sensor Network System for IoT-Enabled Monitoring and Control Systems," *IEEE Internet of Things Journal*, vol. 10, no. 23, pp. 20834–20845, Jun. 2023, doi: 10.1109/JIOT.2023.3284005.
 - [13] H. R. Chowdhury and S. Hussain, "A Compact Quasi-Yagi Microstrip Patch Antenna with High Gain and Bandwidth for UWB Application," *International Journal of Electronics and Telecommunications*, vol. 69, no. 3, pp. 431–437, doi: 10.24425/ijet.2023.144380.
 - [14] M. D. Fernandez, D. Herraiz, D. Herraiz, A. Alomainy, and A. Belenguer, "Design of a Wide-Bandwidth, High-Gain and Easy-to-Manufacture 2.4 GHz Floating Patch Antenna Fed with the Through-Wire Technique," *Applied Sciences*, vol. 12, no. 24, Dec. 2022: 12925, doi: 10.3390/app122412925.
 - [15] L. Y. Nie, B. K. Lau, S. Xiang, H. Aliakbari, B. Wang, and X. Q. Lin, "Wideband design of a compact monopole-like circular patch antenna using modal analysis," *IEEE Antennas and Wireless Propagation Letters*, vol. 20, no. 6, pp. 918–922, Jun. 2021, doi: 10.1109/LAWP.2021.3066985.
 - [16] J. Anguera, A. Andújar, and J. Jayasinghe, "High-directivity microstrip patch antennas based on TM odd-0 modes," *IEEE Antennas and Wireless Propagation Letters*, vol. 19, no. 1, pp. 39–43, Jan 2020, doi: 10.1109/LAWP.2019.2952260.
 - [17] Y. Liu, Y. Jia, W. Zhang, Y. Wang, S. Gong, and G. Liao, "An integrated radiation and scattering performance design method of low-RCS patch antenna array with different antenna elements," *IEEE Transactions on Antennas and Propagation*, vol. 67, no. 9, pp. 6199–6204, Sept. 2019, doi: 10.1109/TAP.2019.2925194.
 - [18] S. H. Abd Hamid, G. C. Hock, and N. Ferdous, "Optimization of Directivity and Gain Performances on Circular Patch Antenna Design for 2.4 GHz Applications," *International Journal of Recent Technology and Engineering*, vol. 8, no. 4, pp. 6442–6447, Nov. 2019, doi: 10.35940/ijrte.D5155.118419
 - [19] N. Ab Wahab, S. A. Nordin, W. N. W. Muhamad, and S. S. Sarnin, "Microstrip rectangular inset-fed patch array antenna for wimax application," in *2020 IEEE International RF and Microwave Conference (RFM)*, IEEE, pp. 1–4, Dec. 2020, doi: 10.1109/RFM50841.2020.9344799.
 - [20] Z. Gan, and Z. H. Tu, "Dual-mode conjoint patch-pair for 5G wideband patch antenna array application," *IEEE Antennas and Wireless Propagation Letters*, vol. 20, no. 2, pp. 244–248, Feb. 2021, doi: 10.1109/LAWP.2020.3046759.
 - [21] P. Bouca, J. N. Matos, S. R. Cunha, and N. B. Carvalho, "Low-profile aperture-coupled patch antenna array for CubeSat applications," *IEEE Access*, vol. 8, pp. 20473–20479, Jan. 2020, doi: 10.1109/ACCESS.2020.2968060.
 - [22] V. Prakasam, K. R. A. LaxmiKanth, and P. Srinivasu, "Design and simulation of circular microstrip patch antenna with line feed wireless communication application," *2020 4th International Conference on Intelligent Computing and Control Systems (ICICCS)* IEEE, Jun. 2020, pp. 279–284, doi: 10.1109/ICICCS48265.2020.9121162.
 - [23] S. Nagaraju, L. Gudino, B. Kadam, V. Khairmar, J. X. Rodrigues, and C. K. Ramesha, "Rectangular microstrip patch antenna array based sectored antenna for directional wireless sensor networks," in *2020 12th International Symposium on Communication Systems, Networks and Digital Signal Processing (CSNDSP)* IEEE, Jul. 2020, pp. 1–6, doi: 10.1109/CSNDSP49049.2020.9249489.
 - [24] K. Mohammed, D. Mehdi, and S. Zeggai, "A 30 GHz Slotted Bow-Tie Rectangular Patch Antenna Design for 5G Application," *International Journal of Electronics and Telecommunications*, vol. 69, no. 4, pp. 669–673, 2023, doi: 10.24425/ijet.2023.147686.
 - [25] G. M. Aji, M. A. Wibisono, and A. Munir, "High gain 2.4 GHz patch antenna array for rural area application," in *2016 22nd Asia-Pacific Conference on Communications (APCC)*, IEEE, Aug. 2016, pp. 319–322, doi: 10.1109/APCC.2016.7581507
 - [26] K. Kaboutari, A. Zabihi, B. Virdee, and M. P. Salmasi, "Microstrip patch antenna array with cosecant-squared radiation pattern profile," *AEU-International Journal of Electronics and Communications*, vol. 106, pp. 82–88, July 2019, doi: 10.1016/j.aeu.2019.05.003.
 - [27] Y. I. Al-Yasir *et al.*, "A new and compact wide-band microstrip filter-antenna design for 2.4 GHz ISM band and 4G applications," *Electronics*, vol. 9, no. 7, p. 1084, Jul. 2020, doi: 10.3390/electronics9071084.
 - [28] M. F. Zambak *et al.*, "A Compact 2.4 GHz L-Shaped Microstrip Patch Antenna for ISM-Band Internet of Things (IoT) Applications," *Electronics*, vol. 12, no. 9, p. 2149, May 2023, doi: 10.3390/electronics12092149.
 - [29] S. G. Fang, S. W. Qu, S. Yang, X. Q. Li, H. B. Sun, and Z. P. Zhou, "Low scattering patch array antenna based on grooved ground," *IEEE Antennas and Wireless Propagation Letters*, vol. 20, no. 3, pp. 308–312, Mar. 2021, doi: 10.1109/LAWP.2020.3048779.
 - [30] M. Alibakhshikenari *et al.*, "Impedance bandwidth improvement of a planar antenna based on metamaterial-inspired T-matching network," *IEEE Access*, vol. 9, pp. 67916–67927, May 2021, doi: 10.1109/ACCESS.2021.3076975.
 - [31] A. Bansal and R. Gupta, "A review on microstrip patch antenna and feeding techniques," *International Journal of Information Technology*, vol. 12 no. 1, pp. 149–154, Mar. 2020, doi: 10.1007/s41870-018-0121-4.
 - [32] C. A. Balanis, "Antenna theory: analysis and design," *John Wiley & Sons*, pp. 816, 2016.
 - [33] M. K. Aghwariya and A. Kumar, "Microstrip patch antenna techniques for wireless applications" in *Microstrip Antenna Design for Wireless Applications*, 1st ed., pp. 3–12, CRC Press, 2021.

BIOGRAPHIES OF AUTHORS






Kymbat Kopbay    was born in 1996. She received the B.S., the M.S. degree in radio engineering, electronics and telecommunications from Al-Farabi Kazakh National University, Almaty, Kazakhstan, in 2017 and 2019, respectively. From 2021, she is a Ph.D. student at the Al-Farabi Kazakh National University. Since 2022, she has been a junior researcher at the Department of Solid-State Physics and Nonlinear Physics. Her research interests include wave propagation, antenna modeling, and wireless sensor networks. She can be contacted at email: kopbay_kymbat2@kaznu.edu.kz.






Madiyar Nurgaliyev    was born in 1994. He received the B.S., the M.S. degree and the Ph.D. degrees in radio engineering, electronics and telecommunications from Al-Farabi Kazakh National University, Almaty, Kazakhstan, in 2016, 2018 and in 2022, respectively. From 2018 to 2022, he was a lecturer at the Department of Solid-State Physics and Nonlinear Physics at the Al-Farabi Kazakh National University. Since 2022, he has been a senior lecturer at the Department of Solid-State Physics and Nonlinear Physics. His research interests include wireless sensor networks, intelligent control systems, and signal processing. He can be contacted at email: nurgaliyev.madiyar@kaznu.kz.






Ahmet Saymbetov    was born in 1982. He received Ph.D. degree in electronics engineering from Physical-Technical Institute of the Academy of Sciences of Uzbekistan, Tashkent, Uzbekistan, in 2011. From 2009 to 2012, he was a senior researcher at the Physical-Technical Institute of the Academy of Sciences of the Republic of Uzbekistan. From 2013 to 2018, he was a senior lecturer with the Department of Solid State Physics and Nonlinear Physics, Al-Farabi Kazakh National University, Almaty, Kazakhstan. Since 2018, he has been an Associate Professor at the Department of Solid State Physics and Nonlinear Physics, Al-Farabi Kazakh National University, Almaty, Kazakhstan. His research interests include wireless sensor networks, intelligent control systems, and information technology. He can be contacted at email: asaymbetov@kaznu.kz.






Nurzhigit Kuttybay    was born in Tulkubas, Kazakhstan in 1993. He received the B.S. in 2015, the M.S. degree in 2017 and the Ph.D. degrees in 2022 in radio engineering, electronics and telecommunications from Al-Farabi Kazakh National University, Almaty, Kazakhstan. Since 2017, he has been a senior lecturer at the Department of Solid-State Physics and Nonlinear Physics at the Al-Farabi Kazakh National University. His research interests include electronics, intelligent control systems, and radio engineering. He can be contacted at email: nurzhigit.kuttybay@kaznu.edu.kz.






Askhat Bolatbek    was born in Almaty, Kazakhstan in 1998. He received the B.S. in 2020, the M.S. degree in 2022 in radio engineering, electronics, and telecommunications from the Almaty University of Power Engineering and Telecommunications named after Gumarbek Daukeyev. Since 2023, he has been studying the Ph.D. degree in radio engineering, electronics, and telecommunications at the Al-Farabi Kazakh National University. Since 2023, he has been working as a lecturer at the Department of Solid-State Physics and Nonlinear Physics at the Al-Farabi Kazakh National University. His research interests include intelligent control systems, wireless sensor networks, electronics, and signal processing. He can be contacted at email: askhat.bolatbek@kaznu.edu.kz.



Sayat Orynbassar    was born in 2000. He received the B.S. in radio engineering, electronics, and telecommunications from the Al-Farabi Kazakh National University in 2022. Since 2022, he is a master's student in electronics and control systems at the Al-Farabi Kazakh National University. His research interests include electronics, intelligent control systems, and information technology. He can be contacted at email: orynbassar_sayat1@kaznu.edu.kz.



Batyrbek Zholamanov    was born in Aral, Kyzylorda, Kazakhstan in 1999. He received the B.S. in 2020, the M.S. degree in 2022 in radio engineering, electronics, and telecommunications from the Al-Farabi Kazakh National University. Since 2022, he has been studying the Ph.D. degree in radio engineering, electronics, and telecommunications at the Al-Farabi Kazakh National University. He was a research assistant at the Department of Solid State Physics and Nonlinear Physics at the Al-Farabi Kazakh National University. Since 2022, he has been working as a lecturer at the Department of Solid State Physics and Nonlinear Physics at the Al-Farabi Kazakh National University. His research interests include intelligent control systems, wireless sensor networks, electronics, and data processing. He can be contacted at email: batyrbek.zholamanov@kaznu.edu.kz.